MONKES: a fast neoclassical code for the evaluation of monoenergetic transport coefficients

F.J. Escoto[1], J.L. Velasco[1], I. Calvo[1], M. Landreman[2] and F.I. Parra[3]

[1]Centro de Investigaciones Energéticas, Medioambientales y Tecnológicas. Avenida Complutense 40, Madrid (Madrid) 28040
[2]University of Maryland, College Park, MD, USA
[3]Princeton Plasma Physics Laboratory, Princeton, NJ 08540, United States of America

E-mail: fjavier.escoto@ciemat.es

April 2023

Abstract.

Keywords: Neoclassical transport, stellarator optimization, bootstrap current.
Submitted to: *Nucl. Fusion*

1. Introduction

2. Drift-kinetic equation and transport coefficients

The new code `MONKES` solves the drift-kinetic equation presented in [1], which is solved by the standard neoclassical code `DKES` [4]. This equation reads

$$(v\xi \boldsymbol{b} + \boldsymbol{v}_E)\cdot\nabla h_a + v\nabla\cdot\boldsymbol{b}\frac{(1-\xi^2)}{2}\frac{\partial h_a}{\partial \xi} - \nu^a \mathcal{L} h_a = S_a, \quad (1)$$

where we have employed as velocity coordinates the cosine of the pitch-angle $\xi := \boldsymbol{v}\cdot\boldsymbol{b}/|\boldsymbol{v}|$ and the module of the velocity $v := |\boldsymbol{v}|$, being $\boldsymbol{B}$ the magnetic field and $\boldsymbol{b} = \boldsymbol{B}/B$ its unitary vector. For the spatial domain we use a system of coordinates in which flux surfaces are assumed to exist and are labelled by $\psi \in [0, \psi_{\rm lcfs}]$ where $\psi_{\rm lcfs}$ denotes the label of the last closed flux surface. The solution to equation (1), h_a, is the deviation of the distribution function from a local Maxwellian

$$f_{{\rm M}a}(\psi, v) = n_a(\psi)\pi^{-3/2}v_{ta}^{-3}(\psi)\exp\left(-\frac{v^2}{v_{ta}^2(\psi)}\right), \quad (2)$$

for the plasma species a of charge e_a, mass m_a, density n_a and temperature T_a (in energy units), where $v_{ta} = \sqrt{2T_a(\psi)/m_a}$ is its thermal velocity. For the convective term in equation (1)

$$\boldsymbol{v}_E = \frac{\boldsymbol{E}_0\times\boldsymbol{B}}{\langle B^2\rangle} = -E_\psi(\psi)\frac{\boldsymbol{B}\times\nabla\psi}{\langle B^2\rangle} \quad (3)$$

denotes the incompressible $\boldsymbol{E}\times\boldsymbol{B}$ drift approximation and $\boldsymbol{E}_0 = E_\psi(\psi)\nabla\psi$ the radial electric field. The prime symbol $'$ denotes a derivative with respect to ψ and the symbol $\langle ...\rangle$ stands for the flux surface average operation. We denote the Lorentz pitch-angle scattering operator by

$$\mathcal{L} = \frac{1}{2}\frac{\partial}{\partial\xi}\left((1-\xi^2)\frac{\partial}{\partial\xi}\right). \quad (4)$$

In the collision operator, $\nu^a(v) = \sum_b \nu^{ab}(v)$ and

$$\nu^{ab}(v) = \frac{4\pi n_b e_a^2 e_b^2}{m_a^2 v_{ta}^3}\log\Lambda\frac{{\rm erf}(v/v_{tb}) - G(v/v_{tb})}{v^3/v_{ta}^3}, \quad (5)$$

stands for the pitch-angle collision frequency between species a and b, we denote the Chandrasekhar function by $G(x) = \left[{\rm erf}(x) - (2x/\sqrt{\pi})\exp(-x^2)\right]/(2x^2)$ and $\log\Lambda$ is the Coulomb logarithm.

The solution of (1) is determined up to a function of (ψ, v) as any function $g(\psi, v)$ belongs to the nullspace of the drift-kinetic equation. This function is unimportant as it does not contribute to the transport coefficients but nevertheless, in order to have a unique solution to the drift-kinetic equation it must be fixed imposing an appropriate additional constraint. We will determine such free function (for fixed (ψ, v)) by imposing

$$\left\langle \int_{-1}^{1} h_a \,{\rm d}\xi \right\rangle = C, \quad (6)$$

for some $C \in \mathbb{R}$.

In the right-hand-side of equation (1)

$$S_a = -\boldsymbol{v}_{{\rm m}a}\cdot\nabla\psi\left(A_{1a} + \frac{v^2}{v_{ta}^2}A_{2a}\right)f_{{\rm M}a} - Bv\xi A_{3a} f_{{\rm M}a}, \quad (7)$$

is the source term,

$$\boldsymbol{v}_{{\rm m}a}\cdot\nabla\psi = -\frac{Bv^2}{\Omega_a}\frac{1+\xi^2}{2B^3}\boldsymbol{B}\times\nabla\psi\cdot\nabla B, \quad (8)$$

is the magnetic radial drift in magnetohydrodynamical equilibrium, $\Omega_a = e_a B/m_a$ is the gyrofrecuency, the flux functions

$$A_{1a}(\psi) = \frac{n_a'}{n_a} - \frac{3}{2}\frac{T_a'}{T_a} - \frac{e_a E_\psi}{T_a}, \quad (9)$$

$$A_{2a}(\psi) = \frac{T_a'}{T_a}, \quad (10)$$

$$A_{3a}(\psi) = -\frac{e_a}{T_a}\frac{\langle \boldsymbol{E}\cdot\boldsymbol{B}\rangle}{\langle B^2\rangle}, \quad (11)$$

are the thermodinamical forces.

Once the equation is solved, taking the moments $\{\boldsymbol{v}_{{\rm m}a}\cdot\nabla\psi, (v^2/v_{ta}^2)\boldsymbol{v}_{{\rm m}a}\cdot\nabla\psi, v\xi B\}$ of h_a and then the flux-surface average yields respectively the radial particle and heat fluxes and the parallel flow

$$\langle \boldsymbol{\Gamma}_a\cdot\nabla\psi\rangle = \left\langle \int \boldsymbol{v}_{{\rm m}a}\cdot\nabla\psi\; h_a \,{\rm d}^3\boldsymbol{v}\right\rangle, \quad (12)$$

$$\left\langle \frac{\boldsymbol{Q}_a\cdot\nabla\psi}{T_a}\right\rangle = \left\langle \int \frac{v^2}{v_{ta}^2}\boldsymbol{v}_{{\rm m}a}\cdot\nabla\psi\; h_a \,{\rm d}^3\boldsymbol{v}\right\rangle, \quad (13)$$

$$\langle n_a \boldsymbol{V}_a\cdot\boldsymbol{B}\rangle = \left\langle B\int v\xi\; h_a \,{\rm d}^3\boldsymbol{v}\right\rangle. \quad (14)$$

It is a common practice in linear neoclassical theory (e.g. [1], [5], [6]) to apply superposition and split h_a in three additive terms, being each one of them a solution to the drift-kinetic equation using as source a summand of (7). Besides, as in the drift-kinetic equation is present the well known monoenergetic approximation (see e.g. [7]), there are no derivatives or integrals along ψ nor v. This approximation permits to use the normalization

$$h_a = f_{{\rm M}a}\left[\frac{Bv}{\Omega_a}\left(A_{1a}f_1 + A_{2a}\frac{v^2}{v_{ta}^2}f_2\right) + A_{3a}f_3\right], \quad (15)$$

relating h_a to three functions $\{f_j\}_{j=1}^3$, which are solutions of

$$\xi \boldsymbol{b}\cdot\nabla f_j + \nabla\cdot\boldsymbol{b}\frac{(1-\xi^2)}{2}\frac{\partial f_j}{\partial \xi} - \frac{\hat{E}_\psi}{\langle B^2\rangle}\boldsymbol{B}\times\nabla\psi\cdot\nabla f_j - \hat{\nu}\mathcal{L}f_j = s_j, \quad (16)$$

for $j=1,2,3$, where $\hat{\nu} := \nu(v)/v$ and $\hat{E}_\psi := E_\psi/v$‡. The source terms are given by

$$s_1 = -\boldsymbol{v}_{\mathrm{m}a}\cdot\nabla\psi\frac{\Omega_a}{Bv^2}, \quad s_2 = s_1, \quad s_3 = -\xi B. \quad (17)$$

The relation between h_a and f_j given by equation (15) is such that the transport quantities (12), (13) and (14) can be written in terms of three transport coefficients which for fixed $(\hat{\nu},\hat{E}_\psi)$ depend only on the magnetic configuration of the flux surface. As $\mathrm{d}\hat{\nu}/\mathrm{d}v$ never annuls, the dependence of f_j on the velocity v can be parametrized by its dependence on $\hat{\nu}$. Thus, for fixed $(\hat{\nu},\hat{E}_\psi)$, equation (16) is completely determined by the magnetic configuration. Hence, its unique solutions f_j that satisfy a condition analogous to (6) are also completely determined by the magnetic configuration.

Using (15) we can write the transport quantities (12), (13) and (14) in terms of the Onsager matrix

$$\begin{bmatrix} \langle \boldsymbol{\Gamma}_a\cdot\nabla\psi\rangle \\ \left\langle \dfrac{\boldsymbol{Q}_a\cdot\nabla\psi}{T_a}\right\rangle \\ \langle n_a\boldsymbol{V}_a\cdot\boldsymbol{B}\rangle \end{bmatrix} = \begin{bmatrix} L_{11a} & L_{12a} & L_{13a} \\ L_{21a} & L_{22a} & L_{23a} \\ L_{31a} & L_{32a} & L_{33a} \end{bmatrix}\begin{bmatrix} A_{1a} \\ A_{2a} \\ A_{3a}\end{bmatrix}. \quad (18)$$

We have defined the thermal transport coefficients as

$$L_{ija} := \int_0^\infty 2\pi v^2 f_{\mathrm{M}a} w_i w_j D_{ija}\,\mathrm{d}v\,, \quad (19)$$

where $w_1 = w_3 = 1$, $w_2 = v^2/v_{\mathrm{t}a}^2$ and we have used that $\int g\,\mathrm{d}^3\boldsymbol{v} = 2\pi\int_0^\infty\int_{-1}^1 g v^2\,\mathrm{d}\xi\,\mathrm{d}v$ for any integrable gyroaveraged function g. The coefficients D_{ija} are the monoenergetic transport coefficients

$$D_{11a} = D_{12a} = D_{21a} = D_{22a} = \frac{B^2v^3}{\Omega_a^2}\widehat{D}_{11}, \quad (20)$$

$$D_{13a} = D_{23a} = \frac{Bv^2}{\Omega_a}\widehat{D}_{13}, \quad (21)$$

$$D_{31a} = D_{32a} = \frac{Bv^2}{\Omega_a}\widehat{D}_{31}, \quad (22)$$

$$D_{33a} = v\widehat{D}_{33}, \quad (23)$$

and $\widehat{D}_{ij}$ are the monoenergetic geometric coefficients given by

$$\widehat{D}_{ij}(\psi,v) = \left\langle \int_{-1}^1 s_i f_j\,\mathrm{d}\xi\right\rangle, \quad i,j\in\{1,2,3\}. \quad (24)$$

‡ The quantity $\hat{\nu}$ is called `CMUL` in the code `DKES`. The quantity $\hat{E}_\psi$ is related to `EFIELD` from `DKES` as `EFIELD` $= \hat{E}_\psi\psi'(r)$ where $r^2/a^2 = \psi/\psi_{\mathrm{lcfs}}$ and a is the minor radius of the device.

Note that, unlike D_{ija}, the monoenergetic geometric coefficients $\widehat{D}_{ij}$ do not depend on the species for fixed $\hat{\nu}$ (however the correspondent value of v associated to each $\hat{\nu}$ varies between species) and depend only on the magnetic geometry. Of the monoenergetic geometric coefficients $\widehat{D}_{ij}$ only three of them are independent as Onsager symmetry implies $\widehat{D}_{13} = -\widehat{D}_{31}$. Hence, to obtain the transport coefficients for all species, requires to solve (16) for two different source terms s_1 and s_3. The algorithm for inverting approximately the left-hand-side of (16) to any degree of accuracy is described in the next section.

3. Numerical method

In this section we describe the algorithm implemented to numerically solve the drift-kinetic equation. As we are not going to do it for a particular source term, but instead a general one, we drop the subscript j that labels every different source term. When we need to distinguish between source terms we will explicitly write their numerical index. Also, as ψ and v act as mere parameters we will omit their dependence in this section and functions of these two variables will be referred as constants. First, in subsection 3.1 we will present the algorithm in a formal and abstract manner which is valid for any set of spatial coordinates. Nevertheless, for convenience, we will explain it in Boozer coordinates (ψ,θ,ζ). The form that relevant magnetic quantities and operators take in these coordinates is listed in Appendix A. The algorithm merges naturally when discretizing the velocity coordinate ξ using a Legendre spectral method. After that, in subsection 3.2 we will explain how, once the coordinates (θ,ζ) are discretized, the algorithm is implemented in `MONKES`.

3.1. Legendre polynomial expansion

The algorithm is based on the approximate representation of the distribution function f in a truncated Legendre series. We will search for approximate solutions to (16) of the form

$$f(\theta,\zeta,\xi) = \sum_{k=0}^{N_\xi} f^{(k)}(\theta,\zeta)P_k(\xi), \quad (25)$$

where $f^{(k)} = \langle f,P_k\rangle_{\mathcal{L}}/\langle P_k,P_k\rangle_{\mathcal{L}}$ is the $k-$th Legendre mode of $f(\theta,\zeta,\xi)$ (see Appendix B) and N_ξ is an integer greater or equal to 1. Of course, in general, the exact solution to (16) does not have a finite Legendre spectrum, but taking N_ξ sufficiently high in expansion (25) would yield an approximate solution to the desired degree of accuracy (in infinite precision arithmetic).

In Appendix B we derive explicitly the projection of each term of (16) onto the Legendre basis when the

representation (25) is used. When doing so, we get that the Legendre modes of the drift-kinetic equation have the tridiagonal representation

$$L_k f^{(k-1)} + D_k f^{(k)} + U_k f^{(k+1)} = s^{(k)}, \qquad (26)$$

for $k = 0, 1, \ldots, N_\xi$, where we have defined for convenience $f^{(-1)} := 0$ and from expansion (25) is clear that $f^{(N_\xi+1)} = 0$. Analogously to (25) we denote the Legendre modes of the source term s by $s^{(k)}$. The spatial differential operators read

$$L_k = \frac{k}{2k-1}\left(\boldsymbol{b}\cdot\nabla + \frac{k-1}{2}\boldsymbol{b}\cdot\nabla \ln B\right), \qquad (27)$$

$$D_k = -\frac{\hat{E}_\psi}{\langle B^2\rangle}\boldsymbol{B}\times\nabla\psi\cdot\nabla + \frac{k(k+1)}{2}\hat{\nu}, \qquad (28)$$

$$U_k = \frac{k+1}{2k+3}\left(\boldsymbol{b}\cdot\nabla - \frac{k+2}{2}\boldsymbol{b}\cdot\nabla \ln B\right). \qquad (29)$$

Thanks to its tridiagonal structure, the system of equations (26) can be formally inverted using the standard Gaussian elimination algorithm for block tridiagonal matrices. Before introducing the algorithm we will explain how to fix the free constant of (26) so that it can be inverted. Note that the aforementioned nullspace of the drift-kinetic equation traduces in the fact that $f^{(0)}$ is not completely determined from (26). To prove this, we inspect the modes $k = 0$ and $k = 1$ that involve $f^{(0)}$. The equation $D_0 f^{(0)} + U_0 f^{(1)}$ is invariant if we add to $f^{(0)}$ any function of $B_\theta(\psi)\zeta + B_\zeta(\psi)\theta$ when $\hat{E}_\psi \neq 0$ and does not include $f^{(0)}$ for $\hat{E}_\psi = 0$. Besides, the equation $L_1 f^{(0)} + D_1 f^{(1)} + U_1 f^{(2)}$ remains invariant if we add to $f^{(0)}$ any constant. Thus, equation (26) is unaltered when we add to $f^{(0)}$ a constant. A condition equivalent to (6) is to fix the value of the $0-$th Legendre mode of the distribution function at a point of the flux-surface. For example,

$$f^{(0)}(0,0) = 0. \qquad (30)$$

With this condition, (26) has a unique solution and can be inverted (further details on the invertibility are given in Appendix C) to obtain an approximation of the first $N_\xi+1$ Legendre modes of the exact solution to (16). The algorithm for formally solving (26) consists of two steps.

(i) **Forward elimination**

Starting from $\Delta_{N_\xi} = D_{N_\xi}$ and $\sigma^{(N_\xi)} = s^{(N_\xi)}$ we can obtain recursively the operators

$$\Delta_k = D_k - U_k \Delta_{k+1}^{-1} L_{k+1}, \qquad (31)$$

and the sources

$$\sigma^{(k)} = s^{(k)} - U_k \Delta_{k+1}^{-1} \sigma^{(k+1)}, \qquad (32)$$

for $k = N_\xi - 1, N_\xi - 2, \ldots, 0$ (in this order). With this procedure we can transform equations (26) to the equivalent system

$$L_k f^{(k-1)} + \Delta_k f^{(k)} = \sigma^{(k)}, \qquad (33)$$

for $k = 0, 1, \ldots, N_\xi$. Note that this process corresponds to perform formal Gaussian elimination over

$$\left[\begin{array}{ccc|c} L_k & D_k & U_k & s^{(k)} \\ 0 & L_{k+1} & \Delta_{k+1} & \sigma^{(k+1)} \end{array}\right], \qquad (34)$$

to eliminate U_k in the first row.

(ii) **Backward substitution**

Once we have the system of equations in the form (33) it is immediate to solve recursively

$$f^{(k)} = \Delta_k^{-1}\left(\sigma^{(k)} - L_k f^{(k-1)}\right), \qquad (35)$$

for $k = 0, 1, ..., N_\xi$ (in this order). Here, we denote by $\Delta_0^{-1}\sigma^{(0)}$ to the solution that satisfies (30). We recall that for $k = 0$, we must impose condition (30) so that $\Delta_0 f^{(0)} = \sigma^{(0)}$ has a unique solution. As $L_1 = \boldsymbol{b}\cdot\nabla$, it is apparent from (35) that the integration constant does not affect the value of $f^{(1)}$.

We can apply this algorithm to solve equation (16) for f_1, f_2 and f_3 to compute approximations to the transport coefficients. In terms of the Legendre modes of f_1, f_2 and f_3, the monoenergetic geometric coefficients read

$$\widehat{D}_{11} = 2\left\langle s_1^{(0)} f_1^{(0)}\right\rangle + \frac{2}{5}\left\langle s_1^{(2)} f_1^{(2)}\right\rangle, \qquad (36)$$

$$\widehat{D}_{31} = \frac{2}{3}\left\langle B f_1^{(1)}\right\rangle, \qquad (37)$$

$$\widehat{D}_{13} = 2\left\langle s_1^{(0)} f_3^{(0)}\right\rangle + \frac{2}{5}\left\langle s_1^{(2)} f_3^{(2)}\right\rangle, \qquad (38)$$

$$\widehat{D}_{33} = -\frac{2}{3}\left\langle B f_3^{(1)}\right\rangle, \qquad (39)$$

where $3s_1^{(0)}/2 = 3s_1^{(2)} = \boldsymbol{B}\times\nabla\psi\cdot\nabla B/B^3$. Note that, in order to compute the monoenergetic geometric coefficients $\widehat{D}_{ij}$ (36), (37), (38) and (39), we only need to calculate the Legendre modes $k = 0, 1, 2$ of the solution and we can stop the backward substitution (35) at $k = 2$. In the next subsection we will explain how `MONKES` approximately solves equation (26) using this algorithm.

3.2. Spatial discretization and algorithm implementation

The algorithm described above allows, in principle, to compute the exact solution to the truncated drift-kinetic equation (26) which is an approximate solution to (16). However, it is not possible, to our knowledge,

to give an exact expression for the operator Δ_k^{-1} except for $k = N_\xi \geq 1$. Instead, we are forced to compute an approximate solution to (26).

Discretizing the θ, ζ coordinates in N_θ and N_ζ equispaced points respectively

$$\theta_i = 2\pi i/N_\theta, \qquad i = 0, 1, \ldots, N_\theta - 1, \tag{40}$$

$$\zeta_j = 2\pi j/(N_\zeta N_p), \qquad j = 0, 1, \ldots, N_\zeta - 1. \tag{41}$$

we can approximate (26) using the Fourier collocation method described in Appendix D and replace (27), (28) and (29) with square matrices of size N_{fs} to obtain the system of equations (D.16). Conceptually, in order to obtain an approximate solution of (26) we assume that each $f^{(k)}$ has a finite Fourier spectrum so that it can be expressed as

$$f^{(k)}(\theta, \zeta) = \boldsymbol{I}(\theta, \zeta) \cdot \boldsymbol{f}^{(k)}, \tag{42}$$

where the interpolant vector map $\boldsymbol{I}(\theta, \zeta)$ is defined at Appendix D and $\boldsymbol{f}^{(k)} \in \mathbb{R}^{N_{\text{fs}}}$ contains $f^{(k)}$ evaluated at the grid points (40), (41). Of course, the exact solution to equation (26) in general has an infinite Fourier spectrum and cannot exactly be written as (42), but taking N_θ and N_ζ sufficiently big, we can approximate the solution to equation (26) to arbitrary degree of accuracy (in infinite precision arithmetic). When $f^{(k)}$ are given by (42), we can obtain a closed system of equations to determine $\boldsymbol{f}^{(k)}$ by evaluating (26) at the grid points (θ_i, ζ_j) and imposing (30). Hence, our approximations $\{f^{(k)}\}_{k=0}^{N_\xi}$ are the unique Fourier interpolants (42) that satisfy the truncated drift-kinetic equation (26) at the nodal points and the nullspace elimination condition (30). To solve approximately (26), one could simply replace in the algorithm the operators L_k, D_k, U_k by the $N_{\text{fs}} \times N_{\text{fs}}$ matrices $\boldsymbol{L}_k$, $\boldsymbol{D}_k$, $\boldsymbol{U}_k$, defined in Appendix D. However, minor modifications to the algorithm, which we will explain, are implemented in `MONKES` in order to be more efficient computationally and in terms of memory resources. Applying (31) yields the matrix $\boldsymbol{\Delta}_k$ for which it requires to invert $\boldsymbol{\Delta}_{k+1}$ and perform at most two matrix multiplications. This inversion takes $O(N_{\text{fs}}^3)$ operations using LU factorization and the matrix multiplications involved aswell. For $k \geq 2$, we can reduce the number of matrix multiplications in determining $\boldsymbol{\Delta}_k$ to 1 if instead of computing $\boldsymbol{\Delta}_{k+1}^{-1}$ we solve for $\boldsymbol{X}_{k+1}$ the matrix system of equations

$$\boldsymbol{\Delta}_{k+1}\boldsymbol{X}_{k+1} = \boldsymbol{L}_{k+1}, \tag{43}$$

and then obtain

$$\boldsymbol{\Delta}_k = \boldsymbol{D}_k - \boldsymbol{U}_k\boldsymbol{X}_{k+1}, \tag{44}$$

for $k = N_\xi - 1, N_\xi - 2, \ldots, 2$. For $k \leq 1$ as we need to solve (33) and do the backward substitution (35), it is convenient to compute and store $\boldsymbol{\Delta}_k^{-1}$. As the resolution of a matricial system of equations and matrix multiplication must be done $N_\xi + 1$ times, the inversion of (D.16) by this method requires $O(N_\xi N_{\text{fs}}^3)$ operations. As we are only interested in the Legendre modes 0, 1 and 2, we do not have to store in memory all the matrices $\boldsymbol{L}_k$, $\boldsymbol{D}_k$, $\boldsymbol{U}_k$ and $\boldsymbol{\Delta}_k$. Instead, we store solely $\boldsymbol{L}_k$, $\boldsymbol{D}_k$, $\boldsymbol{U}_k$ and $\boldsymbol{\Delta}_k^{-1}$ for $k = 0, 1, 2$. For the intermediate steps we just need to use some auxiliary variables $\boldsymbol{L}$, $\boldsymbol{D}$, $\boldsymbol{U}$, $\boldsymbol{\Delta}$ and $\boldsymbol{X}$. Besides, as all the source terms s_i given by (17) do not have Legendre modes greater than 2 we have from equation (32) that $\sigma^{(k)} = 0$ for $k \geq 3$ and $\sigma^{(2)} = s^{(2)}$ and (32) must be applied just for $k = 0$ and $k = 1$. The pseudocode of the implementation of the algorithm in `MONKES` is given in Algorithm 1. In the first loop from $k = N_\xi - 1$ to $k = 2$ we construct $\boldsymbol{L}_2$, $\boldsymbol{\Delta}_2^{-1}$ and $\boldsymbol{U}_2$ without saving any matrix from the intermediate steps nor computing any vector $\boldsymbol{\sigma}^{(k)}$. After that, in the second loop from $k = 1$ to $k = 0$, the matrices $\boldsymbol{L}_k$ and $\boldsymbol{\Delta}_k^{-1}$ are saved for the posterior backward substitution.

Algorithm 1 Block tridiagonal solution algorithm implemented in `MONKES`.

Forward elimination:

- $\boldsymbol{L} \leftarrow \boldsymbol{L}_{N_\xi}$ ▷ Starting value for $\boldsymbol{L}$
- $\boldsymbol{\Delta} \leftarrow \boldsymbol{D}_{N_\xi}$ ▷ Starting value for $\boldsymbol{\Delta}$
- **for** $k = N_\xi - 1$ **to** 2 **do**
  - Solve $\boldsymbol{\Delta}\boldsymbol{X} = \boldsymbol{L}$ ▷ Compute $\boldsymbol{X}_{k+1}$ stored in $\boldsymbol{X}$
  - $\boldsymbol{L} \leftarrow \boldsymbol{L}_k$ ▷ Construct $\boldsymbol{L}_k$ stored in $\boldsymbol{L}$
  - $\boldsymbol{D} \leftarrow \boldsymbol{D}_k$ ▷ Construct $\boldsymbol{D}_k$ stored in $\boldsymbol{D}$
  - $\boldsymbol{U} \leftarrow \boldsymbol{U}_k$ ▷ Construct $\boldsymbol{U}_k$ stored in $\boldsymbol{U}$
  - $\boldsymbol{\Delta} \leftarrow \boldsymbol{D} - \boldsymbol{U}\boldsymbol{X}$ ▷ Construct $\boldsymbol{\Delta}_k$ stored in $\boldsymbol{\Delta}$
  - **if** $k = 2$ **then** ▷ Save required matrices
    - $\boldsymbol{L}_k \leftarrow \boldsymbol{L}$ ▷ Save $\boldsymbol{L}_2$
    - Solve $\boldsymbol{\Delta}\boldsymbol{\Delta}_k^{-1} = \text{Identity}$ ▷ Compute $\boldsymbol{\Delta}_2^{-1}$
    - $\boldsymbol{U}_k \leftarrow \boldsymbol{U}$ ▷ Save $\boldsymbol{U}_2$
  - **end if**
- **end for**
- **for** $k = 1$ to 0 **do**
  - **if** $k > 0$ $\boldsymbol{L}_k \leftarrow \boldsymbol{L}_k$ ▷ Construct and save $\boldsymbol{L}_k$
  - $\boldsymbol{D}_k \leftarrow \boldsymbol{D}_k$ ▷ Construct and save $\boldsymbol{D}_k$
  - $\boldsymbol{U}_k \leftarrow \boldsymbol{U}_k$ ▷ Construct and save $\boldsymbol{U}_k$
  - $\boldsymbol{\Delta}_k^{-1} \leftarrow \boldsymbol{D} - \boldsymbol{U}_k\boldsymbol{\Delta}_{k+1}^{-1}\boldsymbol{L}_k$ ▷ Construct $\boldsymbol{\Delta}_k$
  - $\boldsymbol{\sigma}^{(k)} \leftarrow \boldsymbol{s}^{(k)} - \boldsymbol{U}_k\boldsymbol{\Delta}_{k+1}^{-1}\boldsymbol{\sigma}^{(k+1)}$ ▷ Construct $\boldsymbol{\sigma}^{(k)}$
  - Solve $\boldsymbol{\Delta}\boldsymbol{\Delta}_k^{-1} = \text{Identity}$ ▷ Compute $\boldsymbol{\Delta}_k^{-1}$
- **end for**

Backward substitution:

- $\boldsymbol{f}^{(0)} \leftarrow \boldsymbol{\Delta}_0^{-1}\boldsymbol{\sigma}^{(0)}$
- **for** $k = 1$ **to** 2 **do**
  - $\boldsymbol{f}^{(k)} \leftarrow \boldsymbol{\Delta}_k^{-1}\left(\boldsymbol{\sigma}^{(k)} - \boldsymbol{L}_k\boldsymbol{f}^{(k-1)}\right)$
- **end for**

Once we have solved (D.16) for $\boldsymbol{f}^{(0)}$, $\boldsymbol{f}^{(1)}$ and

$\boldsymbol{f}^{(2)}$, the integrals of the flux surface average operation involved in the geometric coefficients $\widehat{D}_{ij}$ (36), (37), (38) and (39), are conveniently computed using the trapezoidal rule, which for periodic analytic functions has geometric convergence [8]. In the next sections we will see that despite the cubic scaling in N_{fs} of the arithmetical complexity of the algorithm, it is possible to obtain fast and accurate calculations of the monoenergetic geometric coefficients at low collisionality (in particular $\widehat{D}_{31}$) in a single processor. The reason behind this is that in the asymptotic relation $O(N_{\mathrm{fs}}^3) \sim C_{\mathrm{alg}} N_{\mathrm{fs}}^3$, the constant C_{alg} is small enough to allow N_{fs} to take a value sufficiently high to capture accurately the spatial dependence of the distribution function without increasing much the wall-clock time. The algorithm is implemented in the new code `MONKES`, written in Fortran language. The matrix inversion and multiplication are computed using the linear algebra library `LAPACK` [9].

4. Numerical results and benchmark

In this section we will show how `MONKES` provides fast and accurate calculations of the monoenergetic coefficients from low ($\hat{\nu} = 10^{-5}$ m^{-1}) to high collisionality ($\hat{\nu} = 3 \cdot 10^{2}$ m^{-1}) benchmarked with `DKES` and for some cases in which `DKES` are not accurate, also with `SFINCS` [6].

4.1. Convergence of monoenergetic coefficients at low collisionality

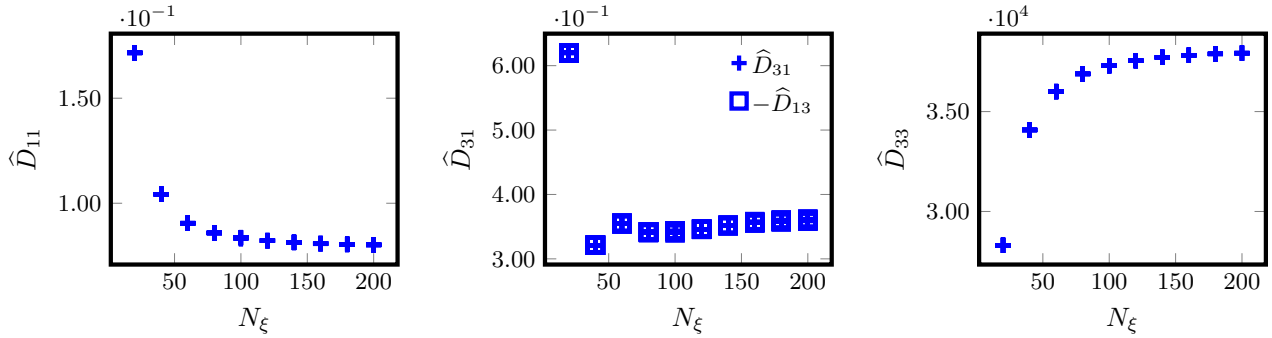

Figure 1: Convergence of monoenergetic coefficients with the number of Legendre modes N_ξ for W7X-EIM at the surface labelled by $\psi/\psi_{\text{lcfs}} = 0.200$, for $\hat{\nu}(v) = 10^{-5}$ m^{-1} and $\hat{E}_r(v) = 0$ kV $\cdot$ s/m^2.

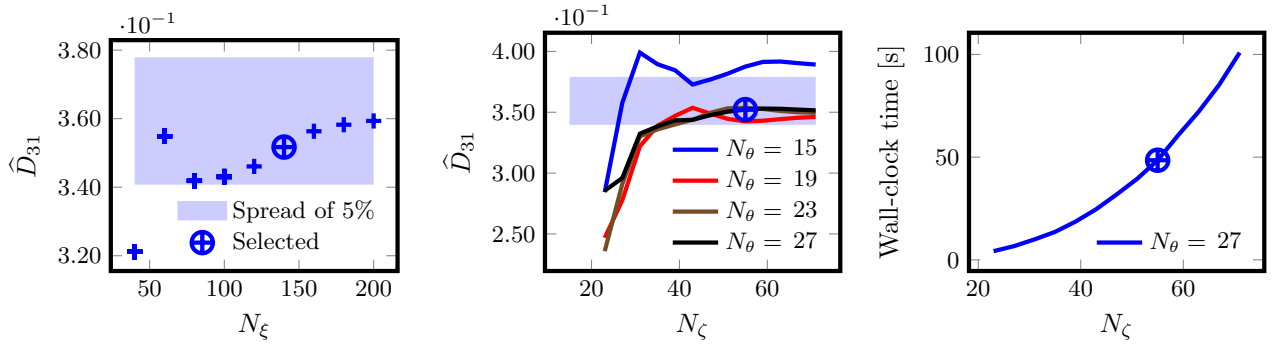

Figure 2: Selection of the resolution to have a sufficiently accurate calculation of the parallel flow geometric coefficient $\hat{\Gamma}_{31}$ for W7X-EIM at the surface labelled by $\psi/\psi_{\text{lcfs}} = 0.200$, for $\hat{\nu}(v) = 10^{-5}$ m^{-1} and $\hat{E}_r(v) = 0$ kV $\cdot$ s/m^2. TO DO: SUBSTITUTE THE CLOCK TIME PLOT.

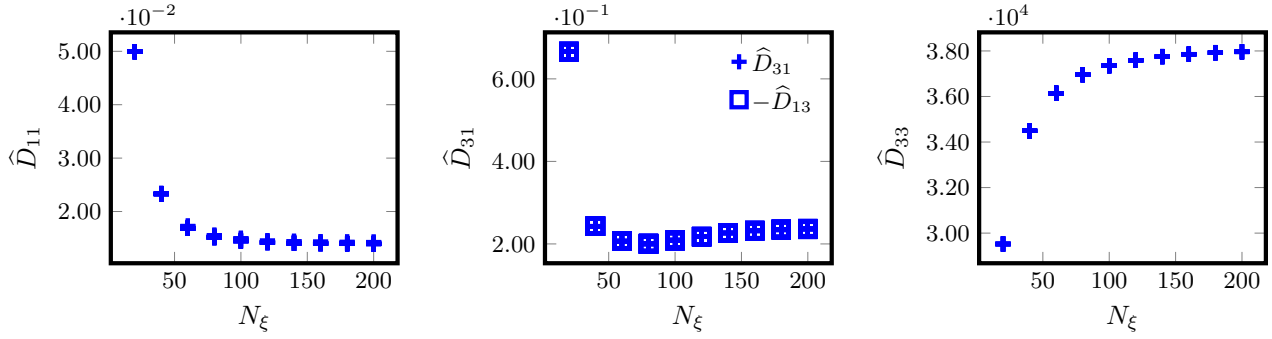

Figure 3: Convergence of monoenergetic coefficients with the number of Legendre modes N_ξ for W7X-EIM at the surface labelled by $\psi/\psi_{\text{lcfs}} = 0.200$, for $\hat{\nu}(v) = 10^{-5}$ m^{-1} and $\hat{E}_r = 3 \cdot 10^{-4}$ kV $\cdot$ s/m^2.

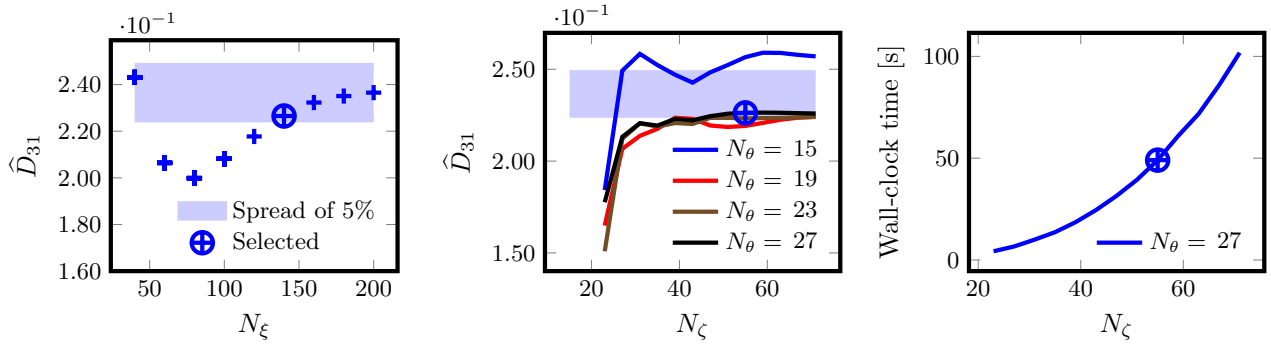

Figure 4: Selection of the resolution to have a sufficiently accurate calculation of the parallel flow geometric coefficient $\hat{\Gamma}_{31}$ for W7X-EIM at the surface labelled by $\psi/\psi_{\text{lcfs}} = 0.200$, for $\hat{\nu}(v) = 10^{-5}$ m^{-1} and $\hat{E}_r(v) = 3 \cdot 10^{-4}$ kV $\cdot$ s/m^2. TO DO: SUBSTITUTE THE CLOCK TIME PLOT.

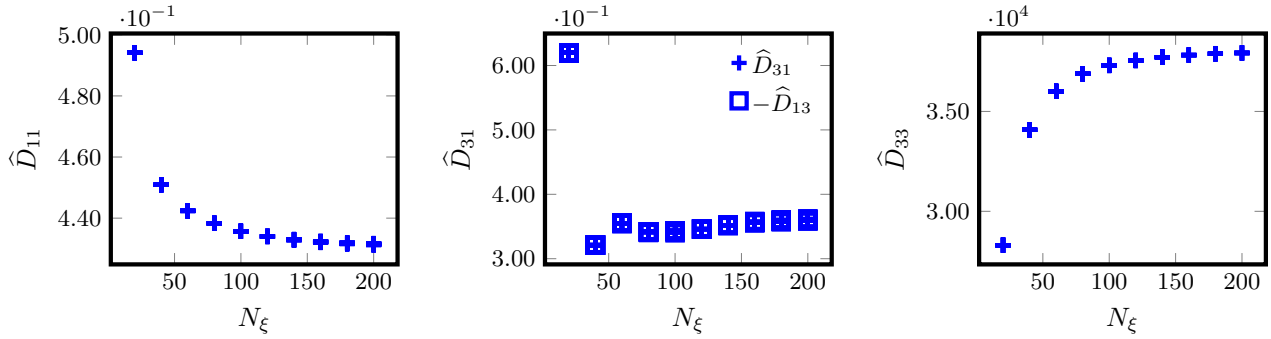

Figure 5: Convergence of monoenergetic coefficients with the number of Legendre modes N_ξ for W7X-KJM at the surface labelled by $\psi/\psi_{\text{lcfs}} = 0.204$, for $\hat{\nu}(v) = 10^{-5}$ m^{-1} and $\hat{E}_r(v) = 0$ kV $\cdot$ s/m^2.

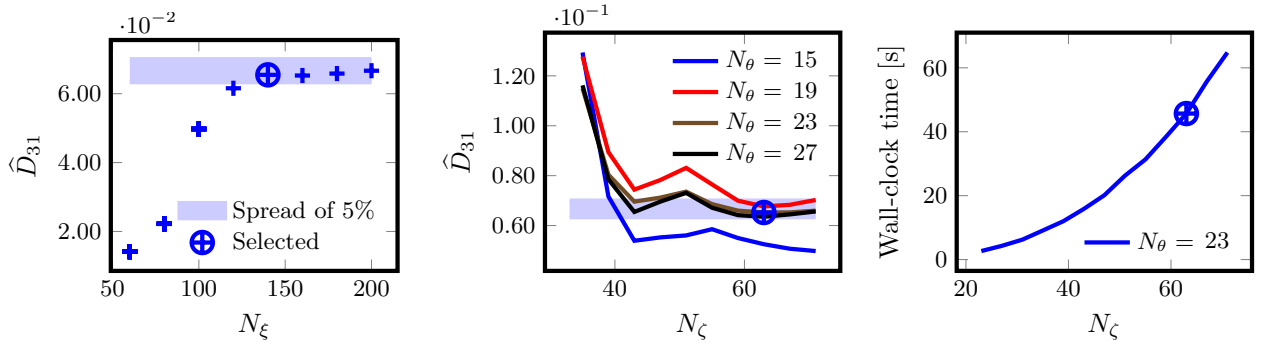

Figure 6: Selection of the resolution to have a sufficiently accurate calculation of the parallel flow geometric coefficient $\hat{\Gamma}_{31}$ for W7X-KJM at the surface labelled by $\psi/\psi_{\text{lcfs}} = 0.200$, for $\hat{\nu}(v) = 10^{-5}$ m^{-1} and $\hat{E}_r(v) = 0$ kV $\cdot$ s/m^2. TO DO: SUBSTITUTE THE CLOCK TIME PLOT AND CHANGE THE THETA ZETA PLOTS.

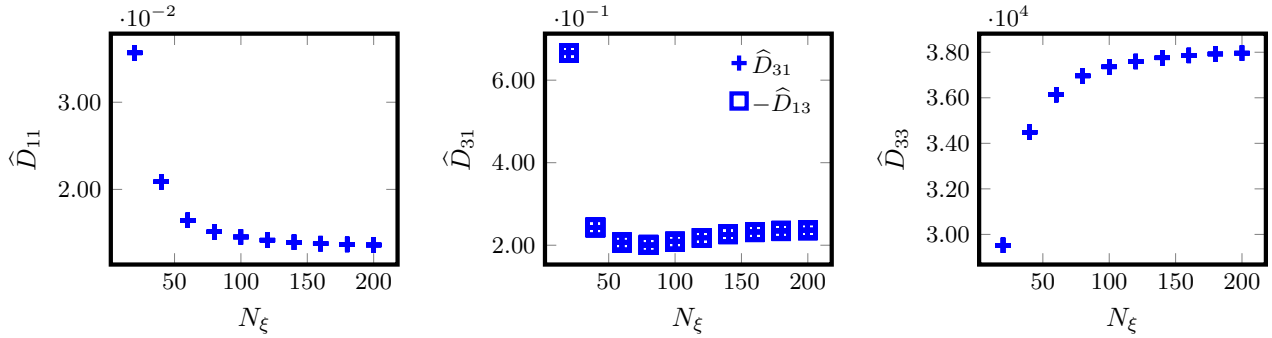

Figure 7: Convergence of monoenergetic coefficients with the number of Legendre modes N_ξ for W7X-KJM at the surface labelled by $\psi/\psi_{\text{lcfs}} = 0.204$, for $\hat{\nu}(v) = 10^{-5}$ m^{-1} and $\hat{E}_r(v) = 3 \cdot 10^{-4}$ kV $\cdot$ s/m^2.

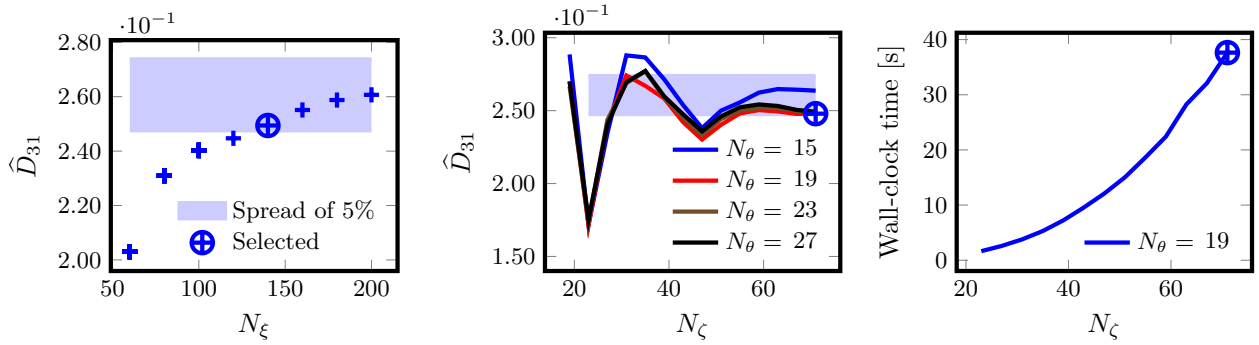

Figure 8: Selection of the resolution to have a sufficiently accurate calculation of the parallel flow geometric coefficient $\hat{\Gamma}_{31}$ for W7X-KJM at the surface labelled by $\psi/\psi_{\text{lcfs}} = 0.200$, for $\hat{\nu}(v) = 10^{-5}$ m^{-1} and $\hat{E}_r(v) = 3 \cdot 10^{-4}$ kV $\cdot$ s/m^2. TO DO: SUBSTITUTE THE CLOCK TIME PLOT AND CHANGE THE THETA ZETA PLOTS.

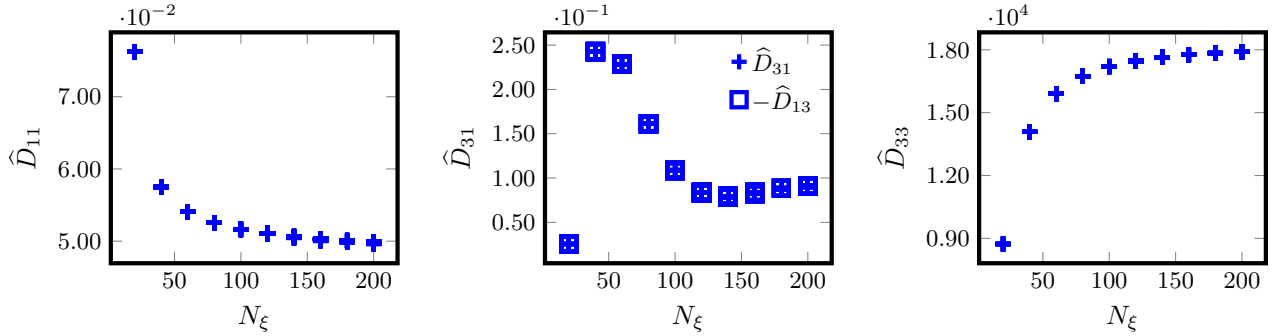

Figure 9: Convergence of monoenergetic coefficients with the number of Legendre modes N_ξ for CIEMAT-QI at the surface labelled by $\psi/\psi_{\text{lcfs}} = 0.25$, for $\hat{\nu}(v) = 10^{-5}$ m^{-1} and $\hat{E}_r(v) = 0$ kV $\cdot$ s/m^2.

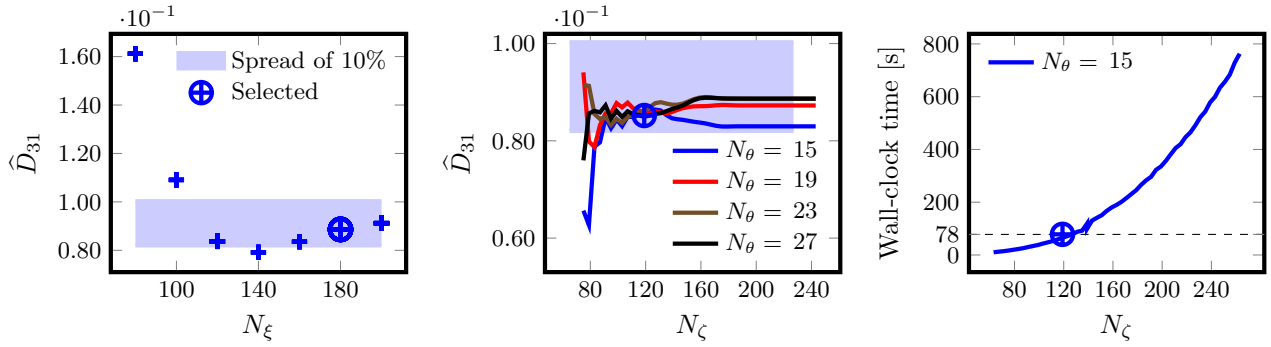

Figure 10: Selection of the resolution to have a sufficiently accurate calculation of the parallel flow geometric coefficient $\hat{\Gamma}_{31}$ for CIEMAT-QI at the surface labelled by $\psi/\psi_{\text{lcfs}} = 0.25$, for $\hat{\nu}(v) = 10^{-5}$ m^{-1} and $\hat{E}_r(v) = 0$ kV $\cdot$ s/m^2.

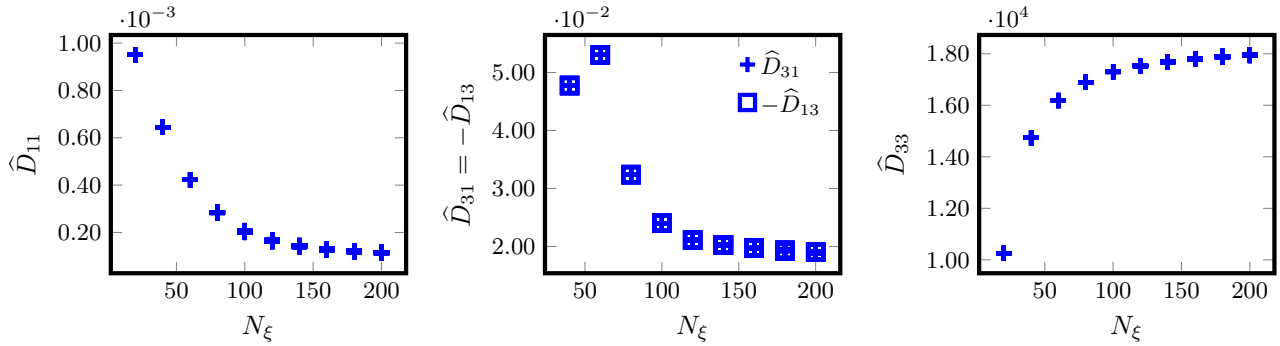

Figure 11: Convergence of monoenergetic coefficients with the number of Legendre modes N_ξ for CIEMAT-QI at the surface labelled by $\psi/\psi_{\text{lcfs}} = 0.25$, for $\hat{\nu}(v) = 10^{-5}$ m^{-1} and $\hat{E}_r(v) = 10^{-3}$ kV $\cdot$ s/m^2.

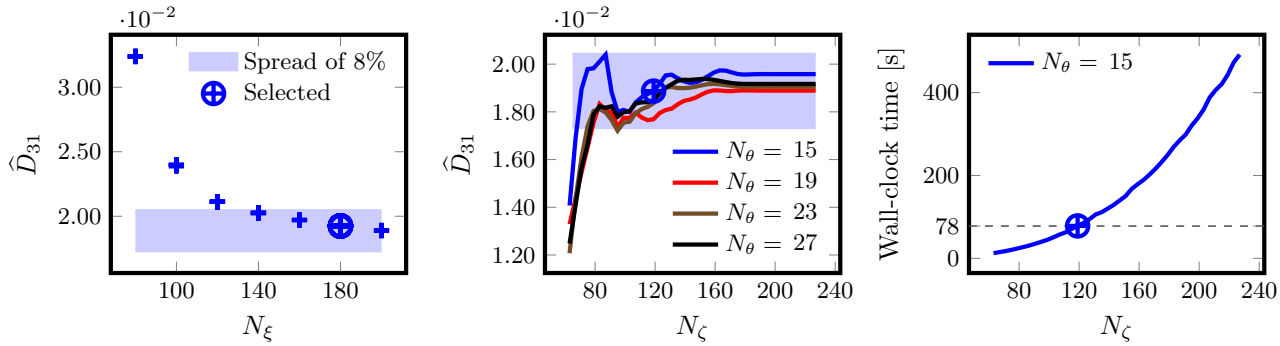

Figure 12: Selection of the resolution to have a sufficiently accurate calculation of the parallel flow geometric coefficient $\widehat{D}_{31}$ for CIEMAT-QI at the surface labelled by $\psi/\psi_{\text{lcfs}} = 0.25$, for $\hat{\nu}(v) = 10^{-5}$ m^{-1} and $\hat{E}_r(v) = 10^{-3}$ kV $\cdot$ s/m^2.

4.2. Benchmark with `DKES`

(i) **Radial transport coefficient**

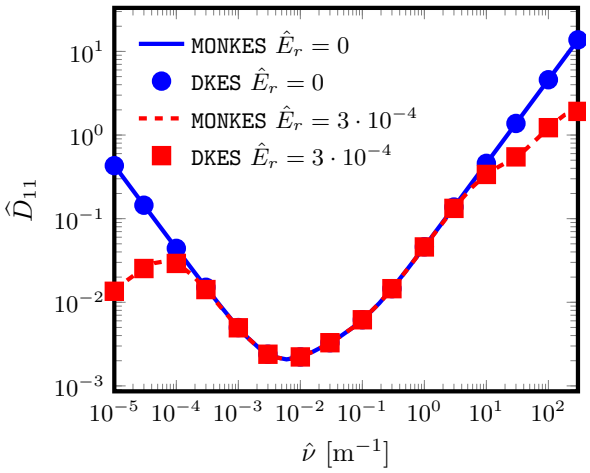

Figure 13: Calculation of $\widehat{D}_{11}$ by `MONKES` and `DKES` in the $1/\nu$ and $\sqrt{\nu}$ regimes for W7-X KJM at the surface $\psi/\psi_{\mathrm{lcfs}} = 0.204$. $\hat{E}_r$ in kV $\cdot$ s/m^2.

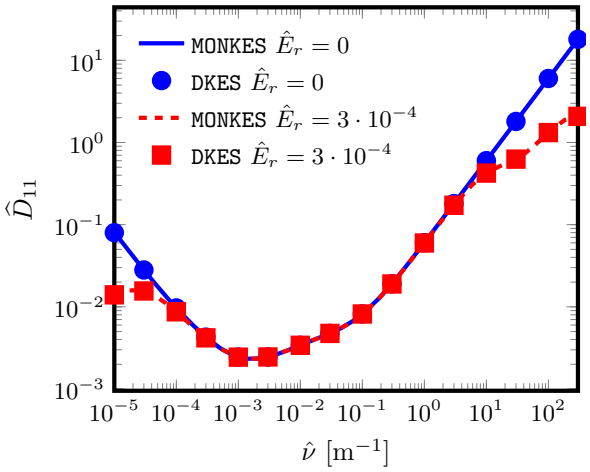

Figure 14: Calculation of $\widehat{D}_{11}$ by `MONKES` and `DKES` in the $1/\nu$ and $\sqrt{\nu}$ regimes for W7-X EIM at the surface $\psi/\psi_{\mathrm{lcfs}} = 0.200$. $\hat{E}_r$ in kV $\cdot$ s/m^2.

(ii) **Parallel flow coefficient**

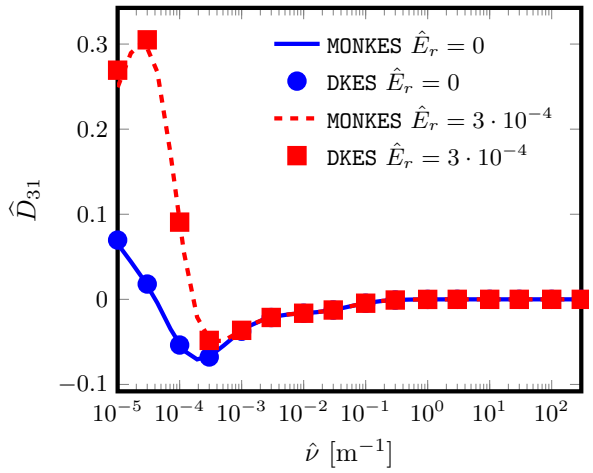

Figure 15: Calculation of $\widehat{D}_{31}$ by MONKES and DKES in the $1/\nu$ and $\sqrt{\nu}$ regimes for W7-X KJM at the surface $\psi/\psi_{\text{lcfs}} = 0.204$. $\hat{E}_r$ in kV $\cdot$ s/m^2.

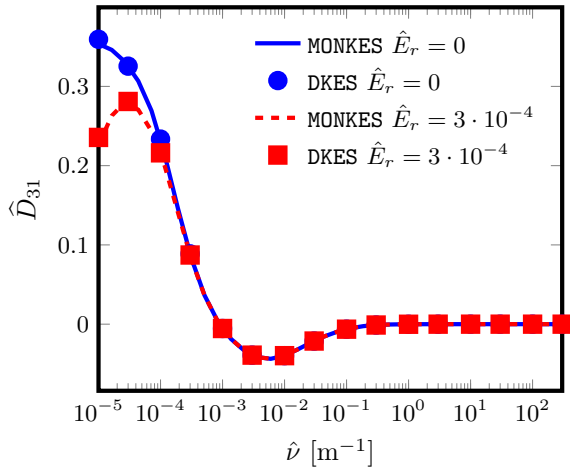

Figure 16: Calculation of $\widehat{D}_{31}$ by MONKES and DKES in the $1/\nu$ and $\sqrt{\nu}$ regimes for W7-X EIM at the surface $\psi/\psi_{\text{lcfs}} = 0.200$. $\hat{E}_r$ in kV $\cdot$ s/m^2.

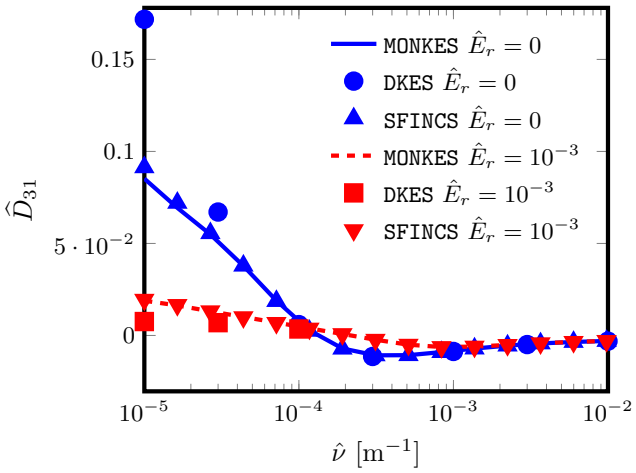

Figure 17: Calculation of $\widehat{D}_{31}$ by MONKES, DKES and SFINCS in the $1/\nu$ and $\sqrt{\nu}$ regimes for CIEMAT-QI EIM at the surface $\psi/\psi_{\text{lcfs}} = 0.250$. $\hat{E}_r$ in kV $\cdot$ s/m^2.

(iii) **Parallel conductivity coefficient**

5. Conclusions

THIS IS JUST A PARAGRAPH CUT AND PASTED FROM OLD STUFF: An important missing feature of the pitch-angle scattering collision operator used in equation (1) is the lack of parallel momentum conservation, i.e. $\int v\xi\nu^a\mathcal{L}F_a\,\mathrm{d}^3\boldsymbol{v}$ is not identically zero. This lack of conservation introduces an spurious parallel force in the macroscopic equation that can be obtained from kinetic equation (1). Hence, the parallel transport predicted by equation (1) is not correct. Fortunately, there exist techniques (see e.g. [10] or [11]) to calculate the parallel transport associated to more accurate momentum conserving collision operators by just solving (1). This has been done successfully in the past by the code `PENTA` [12, 13] which uses the results of `DKES` to compute neoclassical transport with a more refined collision operator that preserves momentum.

Appendices

A. Boozer coordinates

For the spatial domain, in section 3, we will employ right-handed Boozer coordinates $(\psi,\theta,\zeta)\in[0,\psi_{\mathrm{lcfs}}]\times[0,2\pi)\times[0,2\pi/N_p)$. In these coordinates $2\pi\psi$ is the toroidal flux of the magnetic field and θ, ζ are respectively the poloidal and toroidal (in a single period) angles. The integer $N_p\geq 1$ denotes the number of periods of the device. In Boozer coordinates the magnetic field can be written as

$$\begin{aligned}\boldsymbol{B}&=\nabla\psi\times\nabla\theta-\iota(\psi)\nabla\psi\times\nabla\zeta\\&=B_\psi(\psi,\theta,\zeta)\nabla\psi+B_\theta(\psi)\nabla\theta+B_\zeta(\psi)\nabla\zeta,\end{aligned}\quad(A.1)$$

and the Jacobian of the transformation reads

$$\sqrt{g}(\psi,\theta,\zeta):=(\nabla\psi\times\nabla\theta\cdot\nabla\zeta)^{-1}=\frac{B_\zeta+\iota B_\theta}{B^2},\quad(A.2)$$

where we have denoted $B:=|\boldsymbol{B}|$ and $\iota=\boldsymbol{B}\cdot\nabla\theta/\boldsymbol{B}\cdot\nabla\zeta$ is the rotational transform.

Here, the symbol $\langle ...\rangle$ stands for the flux-surface average operation, which in Boozer coordinates (θ,ζ) takes the form

$$\langle F\rangle=\frac{1}{V'(\psi)}\oint\oint\sqrt{g}(\psi,\theta,\zeta)F(\psi,\theta,\zeta)\,\mathrm{d}\theta\,\mathrm{d}\zeta\quad(A.3)$$

for any well-behaved function $F(\psi,\theta,\zeta)$ and $V'(\psi)$ is fixed from the condition $\langle 1\rangle=1$. Also, the spatial differential operators involved in equation (1) in Boozer coordinates take the form

$$\boldsymbol{b}\cdot\nabla=\frac{B}{B_\zeta+\iota B_\theta}\left(\iota\frac{\partial}{\partial\theta}+\frac{\partial}{\partial\zeta}\right),\quad(A.4)$$

$$\boldsymbol{B}\times\nabla\psi\cdot\nabla=\frac{B^2}{B_\zeta+\iota B_\theta}\left(B_\zeta\frac{\partial}{\partial\theta}-B_\theta\frac{\partial}{\partial\zeta}\right).\quad(A.5)$$

B. Legendre modes of the drift-kinetic equation

Legendre polynomials are the eigenfunctions of the Sturm-Liouville problem in the interval $\xi\in[-1,1]$ defined by the differential equation

$$2\mathcal{L}P_k(\xi)=-k(k+1)P_k(\xi),\quad(B.1)$$

where $k\geq 0$ is an integer, and regularity boundary conditions at $\xi=\pm1$

$$(1-\xi^2)\frac{\mathrm{d}P_k}{\mathrm{d}\xi}\bigg|_{\xi=\pm1}=0.\quad(B.2)$$

As $\mathcal{L}$ has a discrete spectrum and is self-adjoint with respect to the inner product

$$\langle f,g\rangle_{\mathcal{L}}:=\int_{-1}^{1}fg\,\mathrm{d}\xi\,,\quad(B.3)$$

in the space of functions that satisfy the regularity condition, $\{P_k\}_{k=0}^{\infty}$ is an orthogonal basis satisfying $\langle P_j,P_k\rangle_{\mathcal{L}}=2\delta_{jk}/(2k+1)$. Hence, these polynomials satisfy the three-term recurrence formula

$$(2k+1)\xi P_k(\xi)=(k+1)P_{k+1}(\xi)+kP_{k-1}(\xi),\quad(B.4)$$

which starting from $P_0=1$ and $P_1=\xi$ defines them all. Additionally, they satisfy the differential identity

$$(1-\xi^2)\frac{\mathrm{d}P_k}{\mathrm{d}\xi}=kP_{k-1}(\xi)-k\xi P_k(\xi).\quad(B.5)$$

Identities (B.4) and (B.5) are useful to represent tridiagonally the Vlasov operator used in (16) when we use the expansion (25). The $k-$th Legendre mode of the term $\xi\boldsymbol{b}\cdot\nabla f$ is expressed in terms of the modes $f^{(k-1)}$ and $f^{(k+1)}$ using (B.4)

$$\begin{aligned}\langle\xi\boldsymbol{b}\cdot\nabla f,P_k\rangle_{\mathcal{L}}=\frac{2}{2k+1}\bigg[&\frac{k}{2k-1}\,\boldsymbol{b}\cdot\nabla f^{(k-1)}\\&+\frac{k+1}{2k+3}\,\boldsymbol{b}\cdot\nabla f^{(k+1)}\bigg].\end{aligned}\quad(B.6)$$

Combining both (B.4) and (B.5) allows to express the $k-$th Legendre mode of the mirror term $\nabla\cdot\boldsymbol{b}((1-\xi^2)/2)\,\partial f/\partial\xi$ in terms of the modes $f^{(k-1)}$ and $f^{(k+1)}$ as

$$\begin{aligned}&\left\langle\frac{1}{2}(1-\xi^2)\nabla\cdot\boldsymbol{b}\frac{\partial f}{\partial\xi},P_k\right\rangle_{\mathcal{L}}=\\&\frac{\boldsymbol{b}\cdot\nabla\ln B}{2k+1}\left[\frac{k(k-1)}{2k-1}f^{(k-1)}-\frac{(k+1)(k+2)}{2k+3}f^{(k+1)}\right],\end{aligned}\quad(B.7)$$

where we have also used $\nabla\cdot\boldsymbol{b} = -\boldsymbol{b}\cdot\nabla\ln B$. The term proportional to $\hat{E}_\psi$ is diagonal in a Legendre representation

$$\left\langle \frac{\hat{E}_\psi}{\langle B^2\rangle}\boldsymbol{B}\times\nabla\psi\cdot\nabla f, P_k\right\rangle_{\mathcal{L}} = \frac{2}{2k+1}\frac{\hat{E}_\psi}{\langle B^2\rangle}\boldsymbol{B}\times\nabla\psi\cdot\nabla f^{(k)}. \tag{B.8}$$

Finally, for the collision operator used in (16), as Legendre polynomials are eigenfunctions of the pitch-angle scattering operator, using (B.1) we obtain the diagonal representation

$$\langle\hat{\nu}\mathcal{L}f, P_k\rangle_{\mathcal{L}} = -\hat{\nu}\frac{k(k+1)}{2k+1}f^{(k)}. \tag{B.9}$$

C. Invertibility of the spatial differential operators

In this Appendix we will study the invertibility of the left-hand-side of (26). For this, we consider L_k, D_k and U_k as operators from the space of smooth functions on the flux-surface $\mathcal{F}$ equipped with the inner product $\langle f,g\rangle_{\mathcal{F}} = \oint\oint fg\,\mathrm{d}\theta\,\mathrm{d}\zeta$ and its induced norm. In this setting L_k, D_k and U_k are bounded operators from $\mathcal{F}$ to $\mathcal{F}$ as all the coefficients are smooth. The operators L_k and U_k given by (27) and (29) do not have a uniquely defined inverse as they have a non zero nullspace. This is a consequence of the fact that the parallel streaming operator

$$\mathcal{V}_\parallel = \xi\boldsymbol{b}\cdot\nabla + \nabla\cdot\boldsymbol{b}\frac{(1-\xi^2)}{2}\frac{\partial}{\partial\xi} \tag{C.1}$$

has a nullspace consisting of functions $g((1-\xi^2)/B)$. Note that we can study the invertibility of L_k and U_k by studying the existence of solutions to

$$\frac{\mathrm{d}h}{\mathrm{d}l} + A(l)h = 0, \tag{C.2}$$

which are not identically zero. Here l is the length along magnetic field lines and $A(l)$ is a smooth function over the flux surface. It is easy to check that

$$h(l) = C_h\exp\left(-\int_0^l A(l')\,\mathrm{d}l'\right), \tag{C.3}$$

where $C_h\in\mathbb{R}$. If $C_h\neq 0$, continuity of h on the torus implies that

$$\int_0^{L_\mathrm{c}} A(l')\,\mathrm{d}l' = 0, \quad \text{if } \iota\in\mathbb{Q} \tag{C.4}$$

$$\lim_{l\to\infty}\int_0^l A(l')\,\mathrm{d}l' = 0, \quad \text{if } \iota\in\mathbb{R}\backslash\mathbb{Q}, \tag{C.5}$$

where L_c is the magnetic field length required for the field line to close itself in a rational surface. On the contrary, if such limit is not 0, C_h must be zero for h to be continuous. Writing the operators L_k and U_k, in the form (C.2) gives $A(l)\propto\partial\ln B/\partial l$, and as $\ln B$ is continuous, either (C.4) or (C.5) is always satisfied. Therefore, the nullspaces of L_k and U_k are not zero, which proves that L_k and U_k are not one-to-one.

Now we will prove that if $\hat{\nu}\neq 0$, all the D_k for $k\geq 1$ are invertible. For $\hat{E}_\psi = 0$, D_k is just a multiplication operator and is obviously invertible if $k\neq 0$. When $\hat{E}_\psi\neq 0$ the proof can be done using a similar argument to the one used for L_k and U_k, as we can transform D_k to an equation superficially very similar to (C.2). First, we change from Boozer angles (ψ,θ,ζ) to a different set of magnetic coordinates $(\tilde{\psi},\alpha,\varphi)$ using the linear transformation

$$\begin{bmatrix}\psi\\ \theta\\ \zeta\end{bmatrix} = \begin{bmatrix}1 & 0 & 0\\ 0 & (1+\iota\delta)^{-1} & \iota\\ 0 & -\delta(1+\iota\delta)^{-1} & 1\end{bmatrix}\begin{bmatrix}\tilde{\psi}\\ \alpha\\ \varphi\end{bmatrix} \tag{C.6}$$

where $\delta = B_\theta/B_\zeta$. In these coordinates $\boldsymbol{B} = \nabla\tilde{\psi}\times\nabla\alpha = B_{\tilde{\psi}}\nabla\tilde{\psi} + B_\varphi\nabla\varphi$ and

$$\boldsymbol{B}\times\nabla\tilde{\psi}\cdot\nabla f = B^2\frac{\partial f}{\partial\alpha}. \tag{C.7}$$

Thus, in coordinates (α,φ), the operator D_k takes the form

$$D_k = -\hat{E}_\psi\frac{B^2}{\langle B^2\rangle}\frac{\partial}{\partial\alpha} + \hat{\nu}\frac{k(k+1)}{2}. \tag{C.8}$$

Hence, we want to prove that

$$-\hat{E}_\psi\frac{B^2}{\langle B^2\rangle}\frac{\partial g}{\partial\alpha} + \hat{\nu}\frac{k(k+1)}{2}g = s(\alpha,\varphi) \tag{C.9}$$

has a unique solution for any source s. The homogeneous and particular solution to this problem are respectively

$$g_\mathrm{h} = G(\varphi)\exp(A_k(\alpha,\varphi)), \tag{C.10}$$

$$g_\mathrm{p} = -\frac{\langle B^2\rangle}{\hat{E}_\psi}\exp(A_k(\alpha,\varphi)) \times\int_0^\alpha s(\alpha',\varphi)\exp(-A_k(\alpha',\varphi))\frac{\mathrm{d}\alpha'}{B^2(\alpha',\varphi)} \tag{C.11}$$

where $G(\varphi)$ is an integration constant and

$$A_k(\alpha,\varphi) = \hat{\nu}\frac{k(k+1)}{2}\frac{\langle B^2\rangle}{\hat{E}_\psi}\int_0^\alpha\frac{\mathrm{d}\alpha''}{B^2(\alpha'',\varphi)}. \tag{C.12}$$

Note from (C.6), that the curves of constant φ are straight lines in the (θ,ζ) plane with slope $-\delta$. This means that there are two options if we follow one of

these curves: if $\delta \in \mathbb{Q}$ it closes itself or if $\delta \in \mathbb{R}\backslash\mathbb{Q}$ it densely fills the whole flux surface. Continuity of $g_{\rm h}$ over the torus implies that in order for $G(\varphi)$ to be non zero, either

$$A_k(L_\alpha, \varphi) = 0, \quad \text{if } \delta \in \mathbb{Q}, \tag{C.13}$$

or

$$\lim_{\alpha\to\infty} A_k(\alpha, \varphi) = 0, \quad \text{if } \delta \in \mathbb{R}\backslash\mathbb{Q}, \tag{C.14}$$

where L_α is the arc-length required for the curve of constant φ to close itself. However, with the exception of A_0 which is identically zero, A_k never annuls. This means that for $k \geq 1$, the constant of integration $G(\varphi)$ in (C.10) is 0. Hence, for $k \geq 1$, we can write the inverse of D_k as the operator

$$D_k^{-1} s = -\frac{\langle B^2 \rangle}{\hat{E}_\psi} \exp(A_k(\alpha, \varphi)) \times \int_0^\alpha s(\alpha', \varphi) \exp(-A_k(\alpha', \varphi)) \frac{\mathrm{d}\alpha'}{B^2(\alpha', \varphi)}, \tag{C.15}$$

and is straightforward to check that $D_k D_k^{-1} s = D_k^{-1} D_k s = s$. The operator D_0 is not invertible as it is identically zero for $\hat{E}_\psi = 0$ and $g_{\rm h} = G(\varphi)$ for $\hat{E}_\psi \neq 0$. Finally, we will study the invertibility of the operator Δ_k

$$\Delta_k = D_k - U_k \Delta_{k+1}^{-1} L_{k+1} \tag{C.16}$$

assuming that Δ_{k+1} is bounded and invertible. For this, first, we note that in the space of functions of interest (smooth periodic functions on the torus), using a Fourier basis $\{e^{\mathrm{i}(m\theta + nN_p\zeta)}\}_{m,n\in\mathbb{Z}}$, we can approximate any function $f(\theta, \zeta) = \sum_{m,n\in\mathbb{Z}} \hat{f}_{mn} e^{\mathrm{i}(m\theta+nN_p\zeta)}$ to arbitrary precision using an approximant $\tilde{f}(\theta, \zeta)$ with $N_{\rm m}$ modes, taking $N_{\rm m}$ sufficiently large. Hence, as they are bounded operators, we can approximate D_k, U_k, Δ_{k+1} and L_{k+1} (and therefore Δ_k) in (C.16) by square matrices of size $N_{\rm m}$. Doing so, we can interpret the matrix representation of Δ_k as the Schur complement of the matrix

$$M_k = \begin{bmatrix} D_k & U_k \\ L_{k+1} & \Delta_{k+1} \end{bmatrix}. \tag{C.17}$$

It is well known from linear algebra that the Schur complement of M_k is invertible when both D_k and Δ_{k+1} are. Hence, for $k \geq 1$, the matrix representation of Δ_k can be inverted for any $N_{\rm m}$, and thus Δ_k is also invertible. For $k = 0$, it is necessary to substitute one of the rows of $[D_k \;\; U_k]$ by the condition (30) so that M_k is invertible for any $N_{\rm m}$ and as Δ_1 can be inverted, also Δ_0 constructed in this way.

D. Fourier collocation method

In this appendix we describe the Fourier collocation (also called pseudospectral) method for discretizing the angles θ and ζ. We define our Fourier interpolant as

$$f^{(k)}(\theta, \zeta) = \boldsymbol{I}(\theta, \zeta) \cdot \boldsymbol{f}^{(k)} = \sum_{j'=0}^{N_\zeta - 1} \sum_{i'=0}^{N_\theta - 1} I_{i'j'}(\theta, \zeta) f^{(k)}(\theta_{i'}, \zeta_{j'}), \tag{D.1}$$

where $\boldsymbol{f}^{(k)} \in \mathbb{R}^{N_{\rm fs}}$ is the state vector containing $f^{(k)}(\theta_{i'}, \zeta_{j'})$. The entries of the vector $\boldsymbol{I}(\theta, \zeta)$ are the functions $I_{i'j'}(\theta, \zeta)$ given by,

$$I_{i'j'}(\theta, \zeta) = I^\theta_{i'}(\theta) I^\zeta_{j'}(\zeta), \tag{D.2}$$

$$I^\theta_{i'}(\theta) = \frac{1}{N_\theta} \sum_{m=-N_{\theta 1}/2}^{N_{\theta 2}/2-1} e^{\mathrm{i}m(\theta-\theta_{i'})}, \tag{D.3}$$

$$I^\zeta_{j'}(\zeta) = \frac{1}{N_\zeta} \sum_{n=-N_{\zeta 1}/2}^{N_{\zeta 2}/2-1} e^{N_p \mathrm{i}n(\zeta-\zeta_{j'})}, \tag{D.4}$$

and $N_{\theta 1} = N_\theta - N_\theta \mod 2$, $N_{\theta 2} = N_\theta + N_\theta \mod 2$, $N_{\zeta 1} = N_\zeta - N_\zeta \mod 2$, $N_{\zeta 2} = N_\zeta + N_\zeta \mod 2$ for some positive integers N_θ, N_ζ. Note that the interpolant is the only finite Fourier sum $\sum_{m=-N_{\theta 1}/2}^{N_{\theta 2}/2-1} \sum_{n=-N_{\zeta 1}/2}^{N_{\zeta 2}/2-1} \tilde{f}_{mn} e^{\mathrm{i}m(\theta-\theta_{i'})} e^{N_p \mathrm{i}n(\zeta-\zeta_{j'})}$ which interpolates the data, as $I^\theta_{i'}(\theta_i) = \delta_{ii'}$ and $I^\zeta_{j'}(\zeta_j) = \delta_{jj'}$. Inserting (D.1) in (26) and evaluating at grid points gives

$$\left(L_k f^{(k-1)} + D_k f^{(k)} + U_k f^{(k)}\right)\Big|_{(\theta_i,\zeta_j)} = \left(L_k \boldsymbol{I} \cdot \boldsymbol{f}^{(k-1)} + D_k \boldsymbol{I} \cdot \boldsymbol{f}^{(k)} + U_k \boldsymbol{I} \cdot \boldsymbol{f}^{(k+1)}\right)\Big|_{(\theta_i,\zeta_j)}. \tag{D.5}$$

Here, $L_k \boldsymbol{I}(\theta_i, \zeta_j)$, $D_k \boldsymbol{I}(\theta_i, \zeta_j)$ and $U_k \boldsymbol{I}(\theta_i, \zeta_j)$ are respectively the rows of $\boldsymbol{L}_k$, $\boldsymbol{D}_k$ and $\boldsymbol{U}_k$ associated to the grid point (θ_i, ζ_j). We can relate them to the actual positions they will occupy in the matrices choosing an ordenation of rows and columns. If we use the ordenation that relates respectively the row $i_{\rm r}$ and column $i_{\rm c}$ to the grid points (θ_i, ζ_j) and $(\theta_{i'}, \zeta_{j'})$ as

$$i_{\rm r} = 1 + i + jN_\theta, \tag{D.6}$$

$$i_{\rm c} = 1 + i' + j'N_\theta, \tag{D.7}$$

for $i, i' = 0, 1, \ldots, N_\theta - 1$ and $j, j' = 0, 1, \ldots, N_\zeta - 1$. With this ordenation we define the elements of the row $i_{\rm r}$ and column $i_{\rm c}$ given by (D.6) and (D.7) of the matrices $\boldsymbol{L}_k$, $\boldsymbol{D}_k$ and $\boldsymbol{U}_k$ to be

$$(\boldsymbol{L}_k)_{i_{\rm r} i_{\rm c}} = L_k I_{i'j'}(\theta_i, \zeta_j), \tag{D.8}$$

$$(\boldsymbol{D}_k)_{i_{\rm r} i_{\rm c}} = D_k I_{i'j'}(\theta_i, \zeta_j), \tag{D.9}$$

$$(\boldsymbol{U}_k)_{i_{\rm r} i_{\rm c}} = U_k I_{i'j'}(\theta_i, \zeta_j). \tag{D.10}$$

Explicitly,

$$L_k I_{i'j'}\Big|_{(\theta_i,\zeta_j)} = \frac{k}{2k-1}\left(\boldsymbol{b}\cdot\nabla I_{i'j'}\Big|_{(\theta_i,\zeta_j)} + \frac{k-1}{2}\,\boldsymbol{b}\cdot\nabla\ln B\Big|_{(\theta_i,\zeta_j)}\delta_{ii'}\delta_{jj'}\right), \tag{D.11}$$

$$D_k I_{i'j'}\Big|_{(\theta_i,\zeta_j)} = \frac{\hat{E}_\psi}{\langle B^2\rangle}\,\boldsymbol{B}\times\nabla\psi\cdot\nabla I_{i'j'}\Big|_{(\theta_i,\zeta_j)} + \frac{k(k+1)}{2}\hat{\nu}\delta_{ii'}\delta_{jj'}, \tag{D.12}$$

$$U_k I_{i'j'}\Big|_{(\theta_i,\zeta_j)} = \frac{k+1}{2k+3}\left(\boldsymbol{b}\cdot\nabla I_{i'j'}\Big|_{(\theta_i,\zeta_j)} + \frac{k+2}{2}\,\boldsymbol{b}\cdot\nabla\ln B\Big|_{(\theta_i,\zeta_j)}\delta_{ii'}\delta_{jj'}\right), \tag{D.13}$$

and

$$\boldsymbol{b}\cdot\nabla I_{i'j'}\Big|_{(\theta_i,\zeta_j)} = \frac{B(\theta_i,\zeta_j)}{B_\zeta+\iota B_\theta} \times\left(\iota\delta_{jj'}\,\frac{\mathrm{d}I^\theta_{i'}}{\mathrm{d}\theta}\Big|_{\theta_i} - \delta_{ii'}\,\frac{\mathrm{d}I^\zeta_{j'}}{\mathrm{d}\zeta}\Big|_{\zeta_j}\right) \tag{D.14}$$

$$\boldsymbol{B}\times\nabla\psi\cdot\nabla I_{i'j'}\Big|_{(\theta_i,\zeta_j)} = \frac{B^2(\theta_i,\zeta_j)}{B_\zeta+\iota B_\theta} \times\left(B_\zeta\delta_{jj'}\,\frac{\mathrm{d}I^\theta_{i'}}{\mathrm{d}\theta}\Big|_{\theta_i} - B_\theta\delta_{ii'}\,\frac{\mathrm{d}I^\zeta_{j'}}{\mathrm{d}\zeta}\Big|_{\zeta_j}\right) \tag{D.15}$$

Thus, we discretize (26) as

$$\boldsymbol{L}_k\boldsymbol{f}^{(k-1)} + \boldsymbol{D}_k\boldsymbol{f}^{(k)} + \boldsymbol{U}_k\boldsymbol{f}^{(k+1)} = \boldsymbol{s}^{(k)}, \tag{D.16}$$

for $k = 0, 1\ldots, N_\xi$. We remark that, for $k = 0$, the rows of $\boldsymbol{D}_0$ and $\boldsymbol{U}_0$ associated to the grid point $(\theta_0,\zeta_0) = (0,0)$, are replaced by equation (30). Each state vector $\boldsymbol{f}^{(k)}$ for the Fourier interpolants contains the images $f^{(k)}(\theta_{i'},\zeta_{j'})$ at the grid points, ordered according to (D.7). Thus, we can solve (D.16) for $\boldsymbol{f}^{(k)}$ applying forward elimination (31) and then backward substitution (35). Finally, we remark that as all $\boldsymbol{f}^{(k)}$ are real, we only need the real part of (D.16).

Acknowledgements

References

[1] S. P. Hirshman, K. C. Shaing, W. I. van Rij, C. O. Beasley, and E. C. Crume. Plasma transport coefficients for nonsymmetric toroidal confinement systems. *The Physics of Fluids*, 29(9):2951–2959, 1986.

[2] Vincent d'Herbemont, Felix I. Parra, Iván Calvo, and José Luis Velasco. Finite orbit width effects in large aspect ratio stellarators. *Journal of Plasma Physics*, 88(5):905880507, 2022.

[3] J.L. Velasco, I. Calvo, F.I. Parra, V. d'Herbemont, H.M. Smith, D. Carralero, T. Estrada, and the W7-X Team. Fast simulations for large aspect ratio stellarators with the neoclassical code knosos. *Nuclear Fusion*, 61(11):116013, sep 2021.

[4] W. I. van Rij and S. P. Hirshman. Variational bounds for transport coefficients in three-dimensional toroidal plasmas. *Physics of Fluids B: Plasma Physics*, 1(3):563–569, 1989.

[5] C.D. Beidler, K. Allmaier, M.Yu. Isaev, S.V. Kasilov, W. Kernbichler, G.O. Leitold, H. Maaßberg, D.R. Mikkelsen, S. Murakami, M. Schmidt, D.A. Spong, V. Tribaldos, and A. Wakasa. Benchmarking of the mono-energetic transport coefficients—results from the international collaboration on neoclassical transport in stellarators (icnts). *Nuclear Fusion*, 51(7):076001, jun 2011.

[6] M. Landreman, H. M. Smith, A. Mollén, and P. Helander. Comparison of particle trajectories and collision operators for collisional transport in nonaxisymmetric plasmas. *Physics of Plasmas*, 21(4):042503, 2014.

[7] Matt Landreman. The monoenergetic approximation in stellarator neoclassical calculations. *Plasma Physics and Controlled Fusion*, 53(8):082003, jun 2011.

[8] Lloyd N. Trefethen and J. A. C. Weideman. The exponentially convergent trapezoidal rule. *SIAM Review*, 56(3):385–458, 2014.

[9] E. Anderson, Z. Bai, C. Bischof, S. Blackford, J. Demmel, J. Dongarra, J. Du Croz, A. Greenbaum, S. Hammarling, A. McKenney, and D. Sorensen. *LAPACK Users' Guide*. Society for Industrial and Applied Mathematics, Philadelphia, PA, third edition, 1999.

[10] M. Taguchi. A method for calculating neoclassical transport coefficients with momentum conserving collision operator. *Physics of Fluids B: Plasma Physics*, 4(11):3638–3643, 11 1992.

[11] H. Maaßberg, C. D. Beidler, and Y. Turkin. Momentum correction techniques for neoclassical transport in stellarators. *Physics of Plasmas*, 16(7), 07 2009. 072504.

[12] D. A. Spong. Generation and damping of neoclassical plasma flows in stellaratorsa). *Physics of Plasmas*, 12(5), 04 2005. 056114.

[13] H. Sugama and S. Nishimura. How to calculate the neoclassical viscosity, diffusion, and current coefficients in general toroidal plasmas. *Physics of Plasmas*, 9(11):4637–4653, 10 2002.